

MULTIWAVELENGTH MONITORING OF THE NARROW-LINE SEYFERT 1 GALAXY AKN 564. III. OPTICAL OBSERVATIONS AND THE OPTICAL–UV–X-RAY CONNECTION

O. SHEMMER,¹ P. ROMANO,² R. BERTRAM,² W. BRINKMANN,³ S. COLLIER,² K.A. CROWLEY,⁴
E. DETSIS,⁵ A.V. FILIPPENKO,⁶ C.M. GASKELL,⁴ T.A. GEORGE,⁴ M. GLIOZZI,³ M.E. HILLER,⁴
T.L. JEWELL,⁴ S. KASPI,¹ E.S. KLIMEK,⁴ M.H. LANNON,² W. LI,⁶ P. MARTINI,^{2,7} S. MATHUR,²
H. NEGORO,⁸ H. NETZER,¹ I. PAPADAKIS,⁵ I. PAPAMASTORAKIS,⁵ B.M. PETERSON,² B.W. PETERSON,⁴
R.W. POGGE,² V.I. PRONIK,⁹ K.S. RUMSTAY,¹⁰ S.G. SERGEEV,⁹ E.A. SERGEEVA,⁹ G.M. STIRPE,¹¹
C.J. TAYLOR,¹² R.R. TREFFERS,⁶ T.J. TURNER,^{13,14} P. UTTLEY,^{15,16} M. VESTERGAARD,² K. VON
BRAUN,¹⁷ R.M. WAGNER,² AND Z. ZHENG²
Received 2001 May 3; accepted 2001 June 28

ABSTRACT

We present the results of a two-year long optical monitoring program of the narrow-line Seyfert 1 galaxy Akn 564. The majority of this monitoring project was also covered by X-ray observations (*RXTE*) and for a period of ~ 50 days, we observed the galaxy in UV (*HST*) and X-rays (*RXTE* & *ASCA*) simultaneously with the ground-based observations. Rapid and large-amplitude variations seen in the X-ray band, on a daily and hourly time-scale, were not detected at optical and UV wavelengths, which in turn exhibited much lower variability either on short (one day) or long (several months) time-scales. The only significant optical variations can be described as two 2–4 day events with $\sim 10\%$ flux variations. We detect no significant optical line variations and thus cannot infer a reverberation size for the broad-line region. Similarly, the large X-ray variations seem to vanish when the light curve is smoothed over a period of 30 days. The UV continuum follows the X-rays with a lag of ~ 0.4 days, and the optical band lags the UV band by ~ 2 days. No significant correlation was found between the entire X-ray dataset and the optical band. Focusing on a 20-day interval around the strongest optical event we detect a significant X-ray–optical correlation with similar events seen in the UV and X-rays. Our data are consistent with reprocessing models on the grounds of the energy emitted in this single event. However, several large X-ray flares produced no corresponding optical emission.

Subject headings: galaxies: active – galaxies: individual (Akn 564) – galaxies: nuclei – galaxies: Seyfert – X-rays: galaxies

1. INTRODUCTION

Narrow-line Seyfert 1 galaxies (NLS1) are a subclass of type 1 Seyfert galaxies defined by their extremely narrow optical permitted emission lines (FWHM $\lesssim 2000$ km s⁻¹) in comparison with normal broad-line active galactic nuclei (AGN; Osterbrock & Pogge 1985). They show extreme AGN properties; their UV-optical emission lines put them at one extreme end of the Boroson & Green (1992) primary eigenvector and they tend to display unusual behavior in other wavebands, especially in

the X-rays. A summary of the properties of NLS1s can be found in Boller, Brandt, & Fink (1996) and Taniguchi, Murayama, & Nagao (1999).

A possible explanation for the narrower emission lines is that NLS1s have relatively low black-hole (BH) masses for their luminosity, but high accretion rates. The broad-line region (BLR) gas location is governed by the luminosity, and the small M_{BH} is responsible for the smaller Keplerian velocities at that location. This hypothesis can be checked observationally by ap-

¹ School of Physics and Astronomy and the Wise Observatory, The Raymond and Beverly Sackler Faculty of Exact Sciences, Tel-Aviv University, Tel-Aviv 69978, Israel; (ohad, netzer, shai)@wise.tau.ac.il

² Department of Astronomy, The Ohio State University, 140 West 18th Avenue, Columbus, OH 43210; (promano, lannon, myana, peterson, pogge, rmw, smita, stefan, zhengz)@astronomy.ohio-state.edu, rayb@as.arizona.edu

³ Max-Planck-Institut für Extraterrestrische Physik, Giessenbachstrasse, 85740 Garching, Germany

⁴ Department of Physics & Astronomy, University of Nebraska, Lincoln, NE 68588-0111; gaskell@unlserve.unl.edu

⁵ Department of Physics, University of Crete, P.O. Box 2208, 71 003 Heraklion, Crete, Greece; jhep@physics.uoc.gr

⁶ Department of Astronomy, University of California, Berkeley, CA 94720–3411; (alex, wli, rtreffers)@astro.berkeley.edu

⁷ Current address: Carnegie Observatories, 813 Santa Barbara St., Pasadena, CA 91101; martini@ociw.edu

⁸ Cosmic Radiation Laboratory, RIKEN, 2-1 Hirosawa, Wako-shi, Saitama 351-01, Japan

⁹ Crimean Astrophysical Observatory, P/O Nauchny, 98409 Crimea, Ukraine and Isaac Newton Institute of Chile, Crimean Branch; (vpronik, sergeev, senena)@crao.crimea.ua

¹⁰ Department of Physics, Astronomy, and Geosciences, Valdosta State University, Valdosta, GA 31698-0055 and the Southeastern Association for Research in Astronomy; krumstay@valdosta.edu

¹¹ Osservatorio Astronomico di Bologna, Via Ranzani 1, I–40127 Bologna, Italy; stirpe@bo.astro.it

¹² Lawrenceville School, PO Box 6008, Lawrenceville, NJ 08648; ctaylor@lawrenceville.org

¹³ Laboratory for High Energy Astrophysics, Code 660, NASA/Goddard Space Flight Center, Greenbelt, MD 20771; turner@lucetia.gsfc.nasa.gov

¹⁴ Joint Center for Astrophysics, Physics Department, University of Maryland Baltimore County, 1000 Hilltop Circle, Baltimore, MD 21250

¹⁵ Department of Physics and Astronomy, University of Southampton, Southampton SO17 1BJ, United Kingdom; pu@astro.soton.ac.uk

¹⁶ Visiting astronomer, Tel-Aviv University, Wise Observatory

¹⁷ Department of Astronomy, University of Michigan, Dennison Building, Ann Arbor, MI 48109; kaspar@astro.lsa.umich.edu

TABLE 1
SUMMARY OF OBSERVATIONS

Observatory	N_{phot}					N_{spec}	Telescope	Instrument	CCD Detector	Resolution
	U	B	V	R	I					
WO	...	60	66	72	...	81	1m	FOSC	Tektronix 1k	$\sim 8 \text{ \AA}$
MDM	20	24	19	18	16	40	1.3m/ 2.4m	CCDS/ MrkIII	Templeton	1.9 \AA (1.3m) 3.4 \AA (2.4m)
CAO	15	2.6m	CCDS	Astro-550- 580x520	8 \AA
KAIT	33	35	32	34	32	...	0.8m	...	SITe 0.5k	...
Loiano	86	1.5m	BFOSC	Loral 2k	...
SARA	...	3	4	3	5	...	0.9m	...	Axiom/Apogee 2k	...
Skinakas	...	59	59	59	59	...	1.3m	...	Tektronix 1k	...
Nebraska	32	0.4m	...	Kodak F-0401	...

plying reverberation mapping techniques to narrow-line AGN, as has been done during the past few years for many AGN. So far, these techniques yielded an estimate of M_{BH} for five type-1 AGN that meet the criterion $\text{FWHM} \lesssim 2000 \text{ km s}^{-1}$: Mrk 335, Mrk 110, NGC 4051, PG 0026+129, and PG 1211+143 (Kaspi et al. 2000; Peterson et al. 2000). These five objects seem to have smaller M_{BH} than other broad-line AGN with similar luminosity (see Figure 7 of Peterson et al. 2000¹⁸), although the statistics are rather poor. Increasing these statistics is a primary goal of this study.

The well-known NLS1 galaxy Arakelian 564 ($z = 0.0247$) is a suitable candidate for a continuous monitoring campaign of this kind. It is one of the brightest NLS1s in X-rays, lies conveniently at a moderate northern declination, and displays many of the extreme properties of the NLS1 class, i.e., $\text{FWHM}(\text{H}\beta) = 700 \text{ km s}^{-1}$, strong Fe II lines, a steep soft-X-ray continuum, and a large soft X-ray excess variance (Turner et al. 1999a). This last property seems to be very common among NLS1s, which show persistent large-amplitude and rapid variability at soft X-ray energies (for an extreme example see the NLS1 galaxy IRAS 13224–3809 where the amplitude of variation reaches a factor of ~ 100 in the X-ray flux; Boller et al. 1997). The nature of these rapid and large-amplitude X-ray variations remains a puzzle and attempts have been made to detect a manifestation of this activity in other bands, mainly in optical wavelengths. The Akn 564 optical monitoring campaign was conducted simultaneously during 1999 with *RXTE* and during 2000 with *HST* (in the UV), *RXTE* and *ASCA* in order to study the relation between the X-ray, UV, and optical variations and to obtain a BH mass for the galaxy using reverberation mapping techniques.

In this paper (Paper III of the series) we present the results of the optical observations of Akn 564 and compare them to the simultaneous X-ray and UV campaigns. The *RXTE* observations are described by Pounds et al. (2001). The *ASCA* and *HST* observations are described in the accompanying papers by Turner et al. (2001) and by Collier et al. (2001), hereafter Papers I and II, respectively. Section 2 presents the ground-based observations and the data reductions. In section 3 we discuss the implications of our results on the nature of NLS1s and on

the optical–UV–X-ray connection in AGN in general. In § 4 we present the conclusions.

2. OBSERVATIONS AND DATA REDUCTION

Akn 564 was observed photometrically and spectrophotometrically from 1998 November through 1999 November and from 2000 May through 2001 January at several ground-based observatories in coordination with the AGN Watch consortium. The following observatories participated in the campaign: Tel-Aviv University Wise Observatory (WO), MDM Observatory at Kitt Peak, Crimean Astrophysical Observatory (CAO), Osservatorio Astronomico di Bologna at Loiano (Loiano), Katzman Automatic Imaging Telescope (KAIT) at Lick Observatory, Observatory of the Southeastern Association for Research in Astronomy (SARA), Skinakas Observatory in Crete, and the University of Nebraska Lincoln Observatory. Table 1 lists the contribution of optical data points by the various observatories. Light curves of the broad-band magnitudes and of the narrow spectral bands, with spectral regions marked on Figure 1, are publicly available in ASCII format at the AGN Watch¹⁹ web page.

Reduction of the data was carried out in the standard way using IRAF²⁰ with its DAOPHOT package for the aperture photometry and its SPECRED, ONEDSPEC, and TWODSPEC packages for the spectroscopic data. Most of the following reduction procedures and methods were described in detail by earlier AGN Watch campaigns (e.g., Kaspi et al. 1996) and we will only repeat them briefly along with the proper references.

Most of the data presented in this paper were obtained at the WO, which defines the reference data set. All other data sets were intercalibrated to the WO data. The spectrophotometric calibration of Akn 564 at the WO is based on observing a nearby comparison star simultaneously with the object of interest in the spectrograph’s wide slit (see Kaspi et al. 2000). Each spectroscopic observation at the WO consisted of two 45 to 60 minute exposures of Akn 564 and its comparison star. The consecutive galaxy/star flux ratio spectra were compared to test for systematic errors in the observations and to reject cosmic rays. We discarded pairs of data points with ratios larger than $\sim 10\%$ and verified that the comparison star is non-variable to within

¹⁸ Two out of seven objects that appear in their analysis, PG 1351+640 and PG 1704+608, have very peculiar lines, formed by a very broad base with a strong superposed narrower core that results in a low FWHM and therefore cannot be considered as NLS1s; see Stirpe (1990) and Boroson & Green (1992).

¹⁹ All publicly available data and complete references to published AGN Watch papers can be found at <http://www.astronomy.ohio-state.edu/~agnwatch>.

²⁰ IRAF (Image Reduction and Analysis Facility) is distributed by the National Optical Astronomy Observatories, which are operated by AURA, Inc., under cooperative agreement with the National Science Foundation.

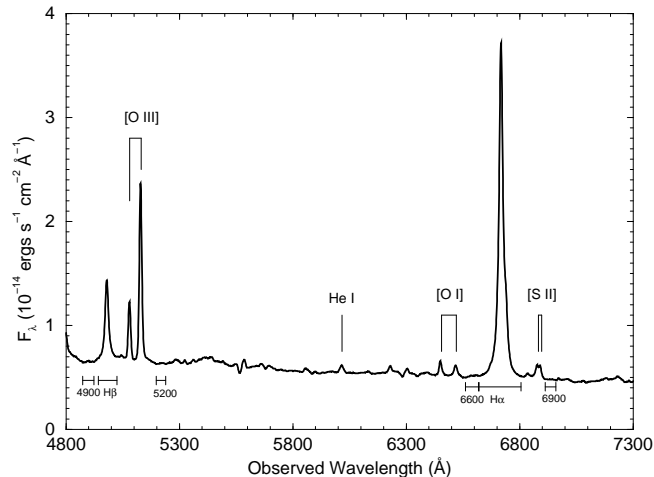


FIG. 1.— Mean spectrum of Akn 564 observed at WO. Continuum and line measurement bins are marked as well as the strongest emission lines.

$\sim 2\%$ by means of differential photometry of other stars in the field (see below). The spectra were calibrated to an absolute flux scale by multiplying each galaxy/star flux ratio spectrum by a flux-calibrated spectrum of the comparison star taken on 1999 January 11, using spectrophotometric standard stars. The absolute flux calibration has an uncertainty of $\sim 10\%$, which is not shown in the error bars of our light curves. The error bars reflect only the relative uncertainties, which are of order 2–3%. In the case of the $H\beta$ light curve, we assigned to the error bars a fixed relative uncertainty that equals the uncertainty in the flux measurements of the [O III] $\lambda 5007$ line (given below) due to the spectral proximity and similar fluxes of the two lines.

Absolute flux calibration of the MDM and CAO spectra was performed by use of spectrophotometric standard stars that were observed each night. The absolute calibration of these spectra was refined by scaling each spectrum to a constant [O III] $\lambda 5007$ flux of $(2.4 \pm 0.1) \times 10^{-13}$ ergs s^{-1} cm^{-2} , which is the mean [O III] $\lambda 5007$ flux measured from the WO spectra. The scaling adjustments to each spectrum were made by using the algorithm of van Groningen & Wanders (1992).

Next, we compared the independent MDM and CAO light curves to the WO light curve in order to identify small systematic flux differences between these data sets (see Peterson et al. 2000 and references therein). We attribute these small relative flux offsets to aperture effects, although the procedure we use also corrects for other unidentified systematic differences between data sets. We define a point-source correction factor φ by the equation

$$F(H\beta)_{\text{WO}} = \varphi F(H\beta)_{\text{observed}}, \quad (1)$$

where $F(H\beta)_{\text{WO}}$ is the reference flux measured for the WO spectra. This factor accounts for the fact that different apertures result in different amounts of light loss for the point-spread function (PSF, which describes the light distribution of the point-like continuum and the broad lines) and the partially extended narrow-line region.

After correcting for aperture effects, another correction needs to be applied to adjust for the different amounts of starlight admitted by different apertures. An extended source correction G is thus defined as

$$F_{\lambda}(5200)_{\text{WO}} = \varphi F_{\lambda}(5200)_{\text{observed}} - G. \quad (2)$$

The value of G is essentially the nominal difference in the con-

TABLE 2
FLUX SCALE FACTORS.

Data Set	Point-Source Scale Factor φ	Extended Source Correction factor G (10^{-14} ergs s^{-1} cm^{-2} \AA^{-1})
MDM (1999)	1.013 ± 0.048	-0.148 ± 0.034
MDM (2000)	0.872 ± 0.040	-0.188 ± 0.023
CAO	0.942 ± 0.055	-0.162 ± 0.012
WO	1	0

taminating host-galaxy flux between the two spectrograph entrance apertures employed. This intercalibration procedure is accomplished by comparing pairs of simultaneous observations from each of the MDM/CAO data sets to that of the WO data set. Since no pairs of WO and MDM/CAO spectra were taken simultaneously, but only with a difference of ~ 0.5 day, we used the interpolation method on the WO data, described by Kaspi et al. (1996), in order to simulate simultaneous pairs. Finally, each MDM/CAO spectrum was multiplied by the average φ and an average G was subtracted from the resultant spectrum (φ and G were averaged among all the close-in-time pairs). The intercalibration constants, φ and G , for each data set are listed in Table 2.

In order to estimate the flux of the AGN component in our spectra, we separated the host galaxy starlight contribution from the nuclear component, by measuring its flux through PSF fitting to field stars in V -band images of the galaxy taken at WO. The subtraction of those PSFs from the images allowed us to find that the host galaxy contributes $\sim 40\%$ to the total light at 5200 \AA . This is a crude estimate, since our limited resolution, governed by a seeing disk of about $2.5''$, does not allow us to separate the various components of the host galaxy, such as a bulge and bar, from the PSF. A constant host contribution of 2.4×10^{-15} ergs s^{-1} cm^{-2} \AA^{-1} was then subtracted from each of the continuum light curves, thus increasing their relative flux uncertainties to the order of $\sim 5\%$ (see Figures 2 & 3).

Photometric data sets for each observatory (except for the Loiano, Skinakas, and Nebraska data sets) and each filter were obtained using the WO DAOSTAT photometric-analysis programme that converted raw IRAF magnitudes of Akn 564 to instrumental magnitudes, relative to a set of reference stars in the galaxy’s field (Netzer et al. 1996). The Loiano data set was reduced separately using the IRAF APPHOT package to measure integrated fluxes for Akn 564 and about 30 field stars. The magnitudes of the stars were used to determine the instrumental magnitudes of the galaxy. The instrumental magnitudes of the Skinakas observations were transformed to the standard system through observations of standard stars from Landolt (1992) during the last four days of their observing run. These observations established a photometric sequence of three reference stars in the field of Akn 564 (Table 3) that was used to transform instrumental magnitudes to the standard system. The Skinakas photometric sequence also enabled transformation of the instrumental magnitudes of Akn 564 from all the other data sets into apparent magnitudes.

3. DISCUSSION

3.1. Optical and X-ray Variability

One of the major goals of this study was to measure the mass of the central BH in Akn 564, which is obtained by cross-correlating continuum and emission line light curves. Unfortunately, throughout the campaign we found no significant correlation between the continuum and the emission lines. This can

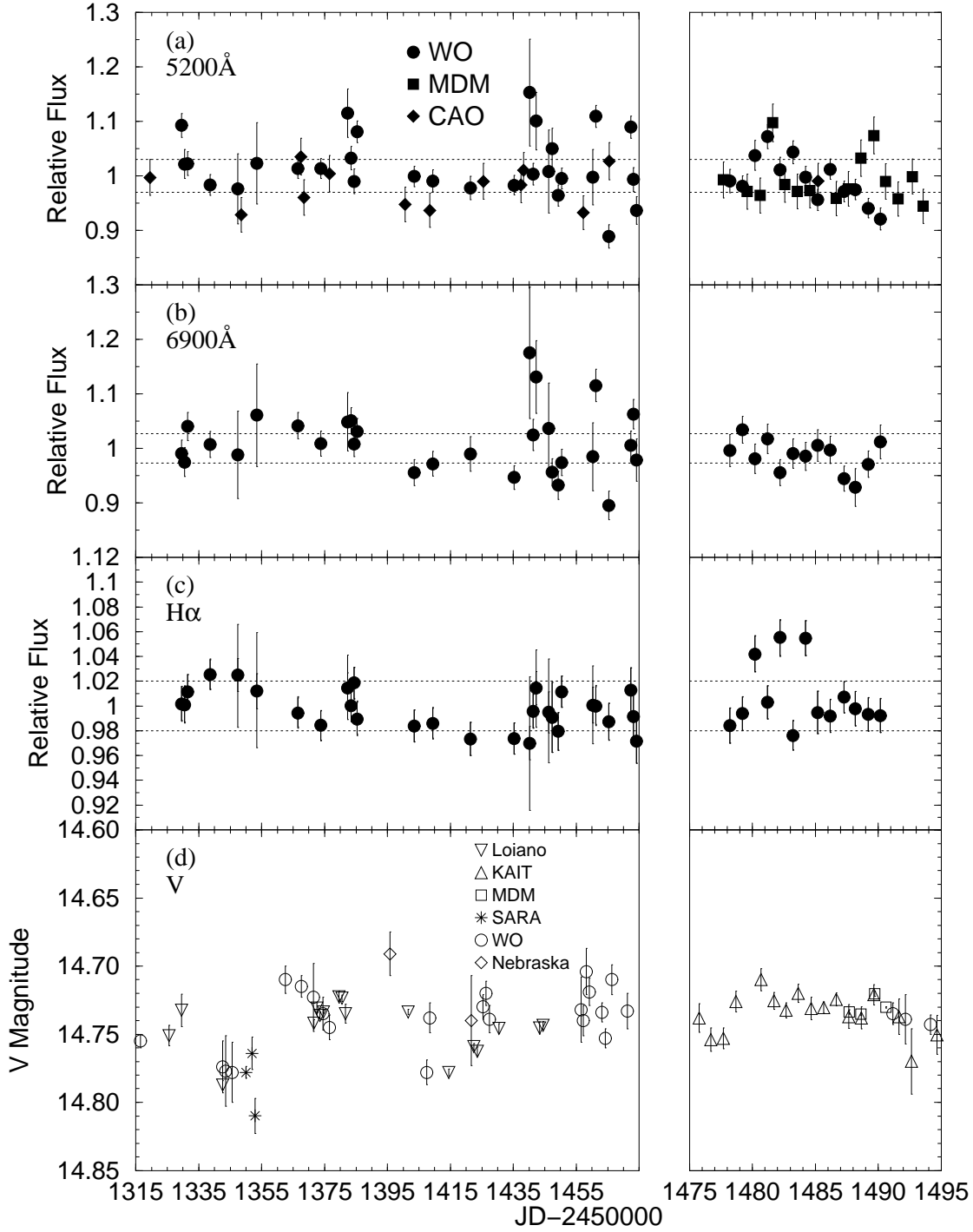


FIG. 2.— Optical light curves of Akn 564 in the 1999 campaign. (a) The continuum at the narrow 5200 Å band. (b) The continuum at the narrow 6900 Å band. (c) H α and (d) V-band (note the different flux scale). Dotted horizontal lines represent $\pm\sigma$ around the mean fluxes. The vertical gap at JD=2451475 defines the beginning of the dense sampling in 1999 (note the different temporal scale to the right of that gap).

be attributed to the fact that H β exhibited only minor variability ($\sim 3\%$) and that H α did not vary significantly.

The fractional variability amplitude F_{var} is defined as

$$F_{var} = \sqrt{\frac{S^2 - \langle \sigma_{err}^2 \rangle}{\langle X \rangle^2}}, \quad (3)$$

where S^2 is the total variance of the light curve, σ_{err}^2 is the mean error squared, and $\langle X \rangle^2$ is the mean flux squared.

This definition is identical to the frequently used excess variance σ_{rms} (Turner et al. 1999a). The uncertainty of F_{var} is (Edelson et al. 2001)

$$\sigma_{F_{var}} = \frac{S^2}{\sqrt{2N} F_{var} \langle X \rangle^2}. \quad (4)$$

Table 4 lists F_{var} values calculated for the optical light curves, and for two X-ray data sets: ASCA 0.7–1.3 keV (Paper I) and

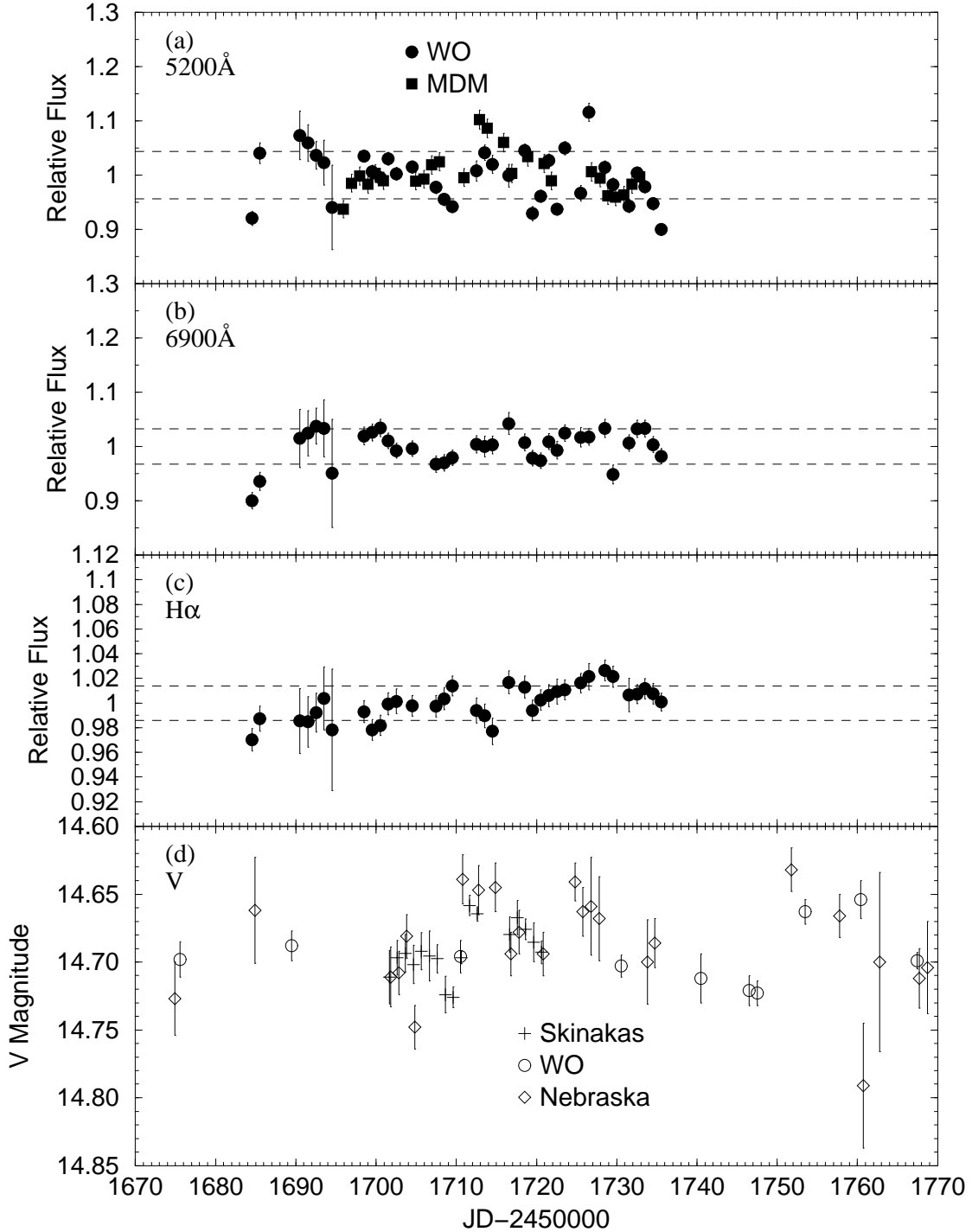


FIG. 3.— Optical light curves of Akn 564 in the 2000 campaign. Symbols and legends are the same as in Figure 2.

RXTE 2–10 keV (Pounds et al. 2001). Although F_{var} depends on the number of data points (equivalent to the length of an observation), it is still possible to compare the excess variance of the X-ray and optical data sets in 1999 and in 2000, since they have roughly the same size. The derived value of F_{var} for the X-rays is about 50% larger than the previously reported value (Turner, George, & Netzer 1999b; see also Paper I). The F_{var} calculated for the optical bands is an order of magnitude smaller than that of the X-rays. By inspection of Figures 2 & 3 and Table 4 it is apparent that the optical light curves, both line

and continua, show negligible variations. At the same time, the X-rays vary rapidly with flux variations as large as 100% throughout the entire monitoring period (see Pounds et al. 2001 and Paper I). The 1999 optical observations show very little ($\sim 3\%$) continuum and line variations compared with typical Seyfert 1 galaxies ($\sim 10\%$) on similar time-scales (e.g., Kaspi et al. 1996; Maoz, Edelson, & Nandra 2000). In 2000 the longer time-scale (several weeks) optical variability continued the 1999 trend, however large-amplitude ($\sim 10\%$) variability on a ~ 1 day time-scale is also observed. The optical varia-

TABLE 3
POSITIONS AND APPARENT MAGNITUDES OF REFERENCE STARS IN THE FIELD OF AKN 564.

Star #	Right Ascension hh:mm:ss (J2000)	Declination dd:mm:ss (J2000)	B	V	R	I
(1)	(2)	(3)	(4)	(5)	(6)	(7)
1	22:42:35.12	29:45:37.56	16.01±0.03	14.77±0.02	14.47±0.02	14.73±0.02
2	22:42:32.08	29:45:26.75	16.34±0.03	15.09±0.02	14.78±0.02	15.03±0.02
3	22:42:39.26	29:44:20.87	14.81±0.03	13.65±0.02	13.37±0.02	13.65±0.02

tions in 2000 can be further compared with the simultaneous UV variations (Paper II), which show a similar trend although with continuum amplitudes almost a factor of two larger.

TABLE 4
FRACTIONAL VARIABILITY F_{var} IN PER CENT

Band	1999 Sparse	1999 Dense	1999 Entire	2000
2–10 keV (<i>RXTE</i>)	25.40±3.19	30.11±4.31	28.36±2.63	33.34±1.71
0.7–1.3 keV (<i>ASCA</i>)	24.23±3.00
4900 Å	4.27±1.05	4.08±1.21	4.31±0.79	4.36±0.64
H β	3.69±1.24	3.18±1.95	3.58±1.02	2.14±1.00
5200 Å	4.05±1.00	3.12±1.13	3.78±0.74	3.88±0.59
6600 Å	2.76±1.29	0.36±3.30	2.39±0.95	1.56±0.70
H α ^a	...	2.10±3.97
6900 Å	3.54±1.30	0.97±1.88	3.26±0.95	1.65±0.75

^aExcept for the 1999 dense-sampling period, F_{var} for H α came out complex since the mean error squared was larger than the variance of the light curve (see equation 3).

3.2. X-ray and UV/Optical Correlations

To derive the cross-correlation function (CCF) between the X-rays (assumed to be the driving light curves) and the UV (from Paper II) and optical continua (assumed to be the responding light curves) we utilized the interpolated CCF (ICCF) method (Gaskell & Sparke 1986), as implemented by White & Peterson (1994), and the Z-transformed discrete correlation function (ZDCF) method (Alexander 1997). The uncertainties on the lags were estimated using the flux randomization/random subset selection (FR/RSS) method (Peterson et al. 1998).

As evident in Paper I, the X-rays are significantly correlated with the UV continuum that follows them with a lag of ~ 0.4 days. We find a similar relation between the soft-X-ray (0.7–1.3 keV from *ASCA*; Paper I) and hard-X-ray bands (2–10 keV from *RXTE*; Pounds et al. 2001) and the UV continuum. Figure 4 shows the CCFs between the two X-ray bands and the continuum at 1365 Å as well as the computed lags and their uncertainties. Both lags are consistent with being larger than zero to at least 68% confidence according to the FR/RSS method.

We have not found any significant correlation between the X-rays and the optical band by correlating the entire data sets (Figure 4c). However, there is an indication that one pronounced event, seen in the X-ray light curves of both *RXTE* and *ASCA*, is also observed in the optical band. This event is clearly seen in Figure 5 as a rise in both the X-ray and optical light curves at JD \approx 2451707, peaks at JD \approx 2451710 (JD \approx 2451713) in X-ray (optical), and then declines rapidly in the X-rays, but more slowly in the optical band. This same pattern is also seen in the simultaneous UV light curves of Akn 564 (Figure 5c; Paper II). Figure 4d shows that when the X-ray and optical narrow-band light curves are truncated to $\sim \pm 10$ days around the peak of

this event, a highly significant correlation, $r = 0.69$, arises with a lag of $1.8^{+0.8}_{-0.7}$ days. We emphasize that other events that are seen in the X-ray light curves, with similar amplitudes, have no detected counterparts in the optical band.

The photometric broad-band data sets were also cross-correlated with the X-rays and UV continua. The results are consistent with those derived with the spectral narrow bands, although the correlations are less significant. In particular, the relatively dense photometric sampling around the optical event, dominated by the Skinakas data set, shows a ~ 1.5 days lag of the optical band relative to the X-rays. Except for the case of this single event, we found no correlation between the optical broad bands and the X-rays.

3.3. Reprocessing Models

As described in § 3.1, the rapid X-ray variations are not detected in the optical and UV bands. A similar relation between the X-rays and the optical band in AGN, i.e., selective response or no response at all of the optical band to the rapid X-ray variations, was recently reported for NGC 3516 (Edelson et al. 2000) and previously reported for two NLS1s: NGC 4051 (Done et al. 1990) and IRAS 13224–3809 (Young et al. 1999), although for the latter, significant optical variations of hourly time-scale were independently found (Miller et al. 2000). However, one event is observed in the light curves of all the bands covered by our campaign. As described in § 3.2, this event appears as a large-amplitude X-ray flare (factor of 3) that rises and declines on a time-scale of ~ 0.5 days, while in the UV and optical bands this flare smears to a small bump on a time-scale of a few days with a much smaller amplitude ($\lesssim 10\%$ change in flux).

Motivated by the single event, we checked whether our data are consistent with reprocessing models in the following ways: 1) by measuring the energy carried by the event across the spectrum, and 2) by comparing the mean energy contained in the 2–10 keV and the 0.7–1.3 keV bands with that contained in the 1365–6900 Å band. We corrected the observed UV/optical spectrum of Akn 564 for Galactic extinction by applying a standard extinction law (Cardelli, Clayton, & Mathis 1989) with $A_B = 0.258$ mag (Schlegel, Finkbeiner, & Davis 1998). Since indications for pronounced reddening in the UV, caused by intrinsic absorbing dust in Akn 564, have been reported in the past (Walter & Fink 1993), we had to correct for intrinsic extinction by comparing the observed He II $\lambda 1640$ /He II $\lambda 4686$ emission-line ratio value of ~ 2.7 with the theoretical value ~ 8 (e.g., Netzer & Davidson 1979) and by assuming linear extinction in λ^{-1} that vanishes at infinite wavelength; in this case $A_B = 0.698$ mag. This way we obtained two different values for the energy of the UV/optical single event and for the mean flux in that band: one that is corrected for standard Galactic extinction, and

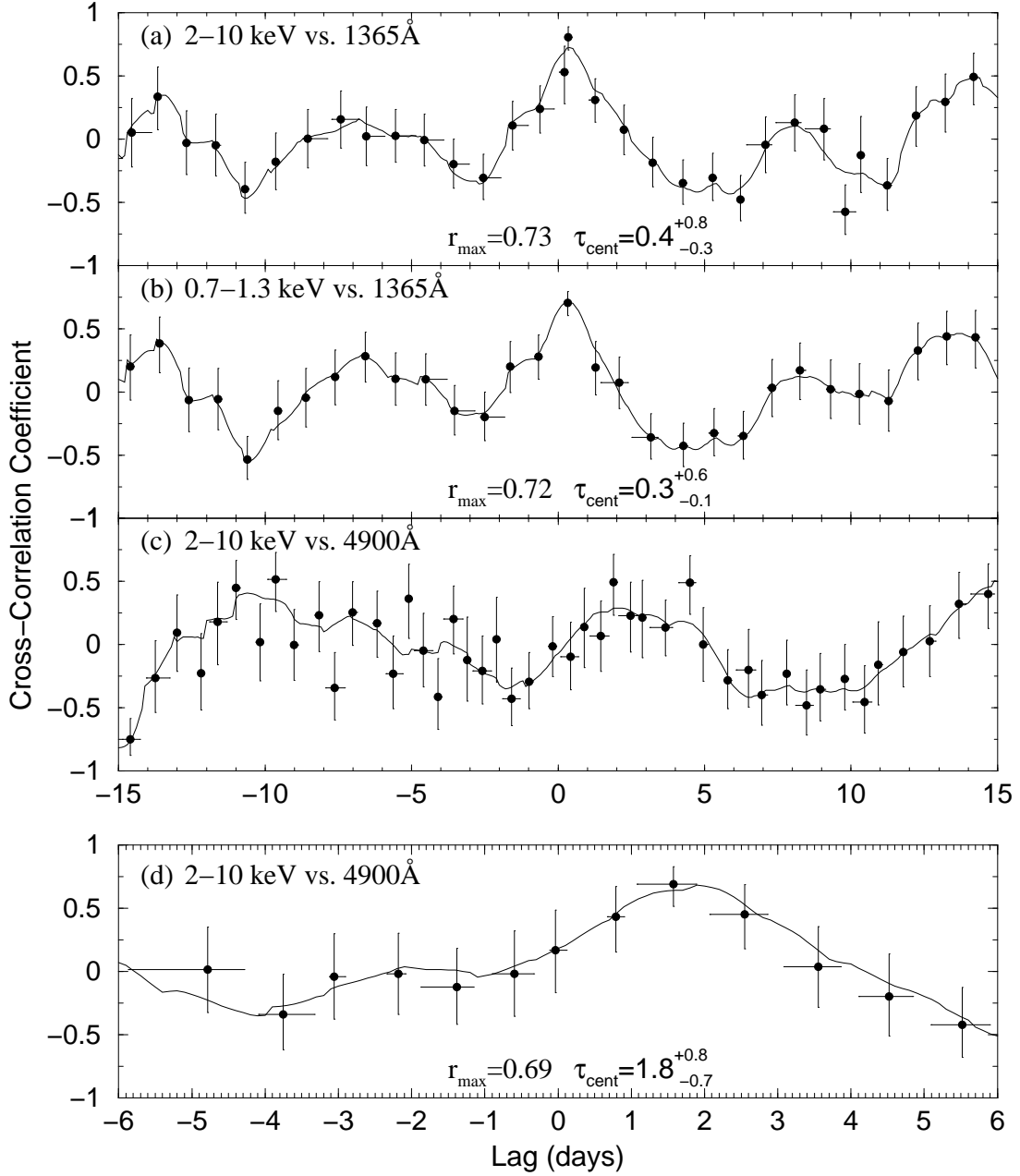


FIG. 4.— Cross-correlation functions. The 2–10 keV band (*RXTE*) and the UV continuum at 1365 Å (*a*), 0.7–1.3 keV band (*ASCA*) and the UV continuum at 1365 Å (*b*), the 2–10 keV band (*RXTE*) and the optical continuum at 4900 Å (*c*) and (*d*). Solid lines and filled circles with error bars represent the ICCF and ZDCF methods, respectively. Positive lags indicate that the second light curve is lagging the first one. The CCF of the 2–10 keV and optical 4900 Å light curves was derived in two different ways: only a portion of the two light curves, covering 20 days and centered on the JD \approx 2451710 event, was considered (*d*), and the entire 2000 May–July light curves were used (*c*). Note the different time-scale in panel (*d*). One can see that a highly significant correlation between the X-rays and optical continuum with a lag of \sim 2 days is dominated by the JD \approx 2451710 event.

the second that also takes into account the effects of intrinsic reddening. We estimated the energy possessed by the event in each band, by approximating its temporal profile to a triangular shape and integrating over time. The mean X-ray fluxes and energy indices were taken from Paper I and the mean UV fluxes of Paper II were used. For $H_0 = 75 \text{ km s}^{-1} \text{ Mpc}^{-1}$ and $q_0 = 0.5$, the energy output during the event reached some 10^{48} ergs in each of the hard-X-ray (2–10 keV), soft-X-ray (0.7–1.3 keV) and UV/optical (1365–6900 Å) bands, corrected for Galactic extinction. The mean flux radiated in the 1365–6900 Å band is $\sim 4 \times 10^{-11} \text{ ergs s}^{-1} \text{ cm}^{-2}$, when corrected for Galactic extinc-

tion, and is comparable to the mean flux in the 0.7–1.3 keV and in the 2–10 keV X-ray bands. On the other hand, the UV/optical (1365–6900 Å) flux increases by almost a factor of 4, when intrinsic reddening is taken into account.

Energy considerations suggest that the case of the X-ray–UV–optical event of JD \approx 2451710, corrected only for Galactic extinction, is consistent with reprocessing models. In such models it is assumed that the X-rays and the UV/optical band are strongly coupled, since an X-ray continuum source irradiates a relatively dense and cool absorbing medium and the energy of the absorbed X-rays is then re-radiated at longer wave-

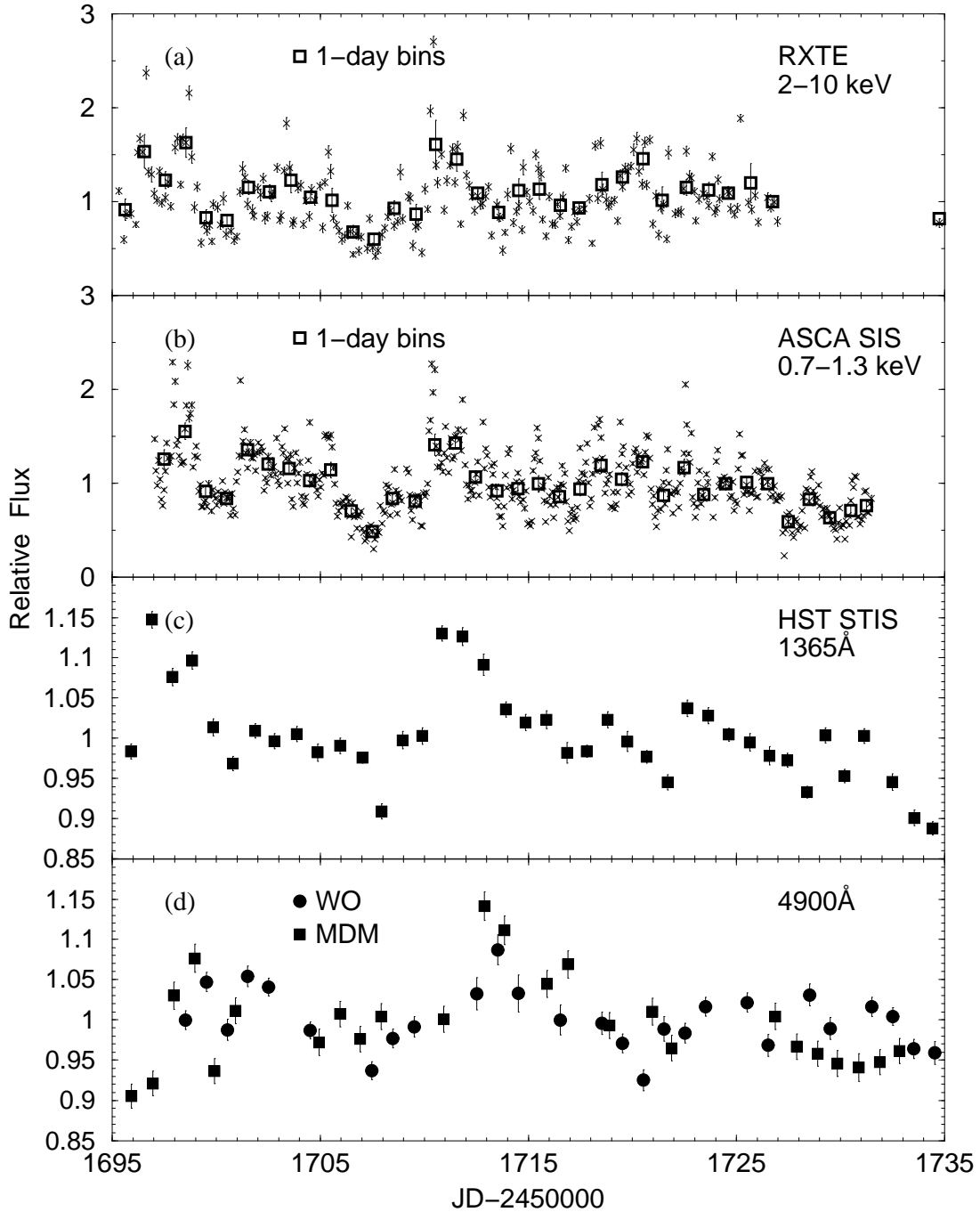


FIG. 5.— Closeup view of the $\text{JD} \approx 2451710$ event common to the X-ray (a) and (b), UV (c) and optical (d) light curves. Empty squares in the X-ray light curves represent 1-day binning of the data.

lengths. However, when the UV/optical band is corrected for intrinsic reddening, the mean flux in that band is larger than the combined flux in the 0.7–1.3 and 2–10 keV X-ray bands by a factor of two, implying that there is not enough X-ray energy to account for the intrinsic UV/optical single event and mean flux. Obviously, the above numbers depend, to a large extent, on the exact energy range considered for the seed photons. Therefore, the reprocessing interpretation of the single event should be considered with caution, depending on the participating energy ranges as well as on the properties and geometry of the intrinsic extinction.

Our data imply that it takes an X-ray pulse that covers ~ 0.4 days in time, ~ 0.4 days to appear in the UV band and then, ~ 2 days later on, to appear in the optical band as well. In both the UV and optical light curves, this pulse extends to a time-scale of about 4 days. A simple interpretation of this scenario suggests that the region from which the variable portion of the UV/optical flux is emitted has a size of about 4 light days and is 0.4–2 light days distant from the X-ray source. The inferred minimal distance of 0.4 light days, corresponding to the delayed UV response (with respect to the X-rays), can be compared with various theoretical size estimates. For a thin accre-

tion disk, most of the UV flux is emitted within $\sim 30R_g$ (gravitational radii). Comparing the two suggests $M_{\text{BH}} \gtrsim 10^8 M_\odot$, more than an order of magnitude larger than the $10^7 M_\odot$ estimate of Pounds et al. (2001), which is based on a power density spectrum (PDS) analysis. Thus the size of the reprocessing region is much larger than the size of the internally produced UV radiation, which is what we expect. Mass estimates based on slim accretion disk models, perhaps more appropriate to the case of NLS1s, are in closer agreement with the Pounds et al. (2001) estimate, since they are associated with higher temperatures and larger UV emitting regions (Abramowicz et al. 1988; Mineshige et al. 2000).

The main difficulty with the reprocessing scenario is the observational evidence that, at most times, the bulk of the optical emission does not respond to the X-ray variations, which occur mainly on very short time scales ($\lesssim 1$ day). It has been suggested that the physical nature of the rapid X-ray variations is associated with localized flaring activity (Stern et al. 1995). Such X-ray activity may arise in the corona above the accretion disk. Alternatively, this activity may be a consequence of relativistic boosting as described by Young et al. (1999) and Boller et al. (1997), such that the X-rays always have a boost factor which is many times larger than the optical boost factor. The flaring activity may also be associated with the disk itself, where magnetic flares produce large fluctuations in magnetic-field energy release (Mineshige et al. 2000 and references therein). These explanations are consistent with the case of Akn 564 because of the absence of an X-ray–optical correlation, except for the single event. In this case there might be multiple continuum regions that do not all participate in the reprocessing, perhaps due to unusual geometry.

There is growing evidence that the key to the relationship between the optical and X-ray bands lies in the longer time-scales, i.e., months to years. A possible 100-day lag of the X-rays over the optical band (leading band) for NGC 3516 was recently reported by Maoz et al. (2000), who suggested that the X-rays are possibly emitted by two different components/mechanisms, where one is exhibiting short time-scale behavior (i.e., the flaring activity) which is not reflected in the optical band, while the other exhibits long time-scale variations, which are possibly correlated with the optical band. A similar case applies for NGC 4051 (Peterson et al. 2000), where the long time-scale variations of both the X-ray and optical bands are seen to be correlated, although with zero lag. In order to look for large time-scale trends in the X-ray light curves, we smoothed the *RXTE* X-ray data with boxcars ranging from 10 to 30 days, similar to what was done for NGC 4051 (Peterson et al. 2000) and for NGC 3516 (Maoz et al. 2000). The rapid X-ray variations are suppressed to $\sim 30\%$ when a smoothing boxcar of 20 days is applied and almost disappear when a boxcar of 30 days is used (see Figure 6). This behavior is also reflected in the PDS of the X-ray variations recently calculated by Pounds et al. (2001). These authors report that the turn-over frequency in the PDS corresponds to ~ 13 days, which implies that most of the X-ray variability of Akn 564 occurs on the order of these time-scales or smaller. The results presented in this paper show that for Akn 564, on a long time-scale (months to years) during this campaign, both the X-rays and the optical bands did not vary.

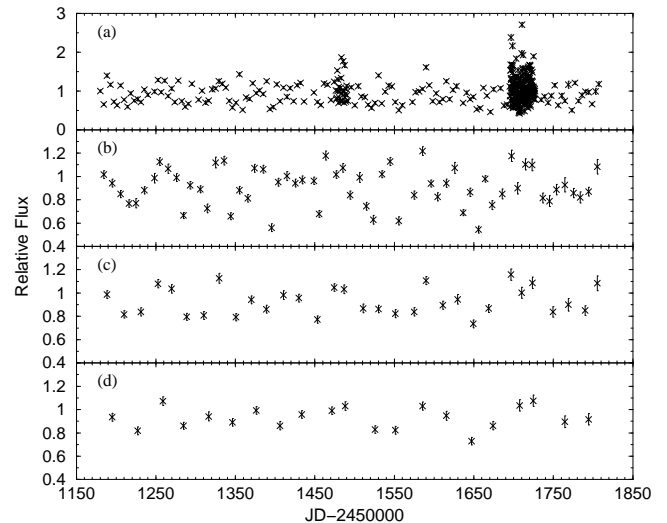


FIG. 6.— Original and smoothed X-ray light curves. The original *RXTE* light curve (a) was binned by 10, 20, and 30 days; the resulting light curves appear in panels (b), (c), and (d), respectively. Note the large difference in flux scale between the original and the smoothed light curves.

4. CONCLUSIONS

This paper reports the results of the optical monitoring campaign on the NLS1 galaxy Akn 564. During this campaign Akn 564 was observed in X-rays with *RXTE*, continuously with a varying sampling rate from 1999 January 1 until 2000 September 19, and with *ASCA* continuously from 2000 June 1 until 2000 July 5. The optical observations were made in the 1998–1999, 1999–2000, and 2000–2001 seasons with sampling rates varying from once a week to twice a day. In 2000 May–July, Akn 564 was also observed in the UV with *HST*, with a sampling rate of ~ 1 day. Our observational results are incorporated with some of the main findings of Turner et al. (2001) and Collier et al. (2001) to produce a complete multiwavelength picture that emerges from this campaign, as follows:

1. The very strong (a factor of 2–3 peak-to-peak) and rapid ($\lesssim 1$ day) X-ray variations that characterize NLS1 galaxies are also seen in Akn 564. The mean X-ray flux was basically constant on time-scales larger than ~ 30 days, similar to the mean UV and optical flux.
2. Most emission lines did not show any significant variation. $\text{Ly}\alpha$ and $\text{N V } \lambda 1240$ exhibit at most $\sim 7\%$ full range flux variations mainly during two short occasions. This prevented us from measuring accurately the broad-line region size and the central black-hole mass. However, there is evidence for correlated $\text{Ly}\alpha$ -continuum variability which is consistent with $\lesssim 3$ days lag and can be used to derive a mass estimate of $\lesssim 8 \times 10^6 M_\odot$.
3. The total flux in the soft X-ray band is well-correlated with the hard X-ray flux, with zero lag.
4. The UV continuum follows the X-rays with a lag of ~ 0.4 days.

5. The detected wavelength-dependent UV/optical continuum time delays can be considered as evidence for a stratified continuum reprocessing region, possibly an accretion-disk structure. The 4900 Å continuum band lags the 1365 Å continuum by ~ 1.8 days.
6. The optical continuum is not significantly correlated with the X-rays. However, focusing on a 20-day period around the largest optical event gives a significant correlation with a lag of ~ 2 days.
7. Our data are consistent with reprocessing models on the grounds of a single flare that was observed in all wavelengths. However, other X-ray flares do not produce corresponding UV/optical continuum emissions.

We are grateful to WO staff members Ezra Mashal, Friedel Loinger, Sammy Ben-Guigui, and John Dann for their crucial contribution to this project. Astronomy at the WO is supported by a long-term grant from the Israel Science Foundation. The MDM observations were supported through grants to Ohio State University from the NSF through grant AST-9420080 and by NASA through grant HST-GO-08265.01-A from the Space Telescope Science Institute, which is operated

by the Association of Universities for Research in Astronomy, Inc., under NASA contract NAS5-26555. The KAIT observations are supported by NSF grant AST-9987438, as well as by the Sylvia and Jim Katzman Foundation. The CAO observations were supported by Award No. UP1-2116 of the U.S. Civilian Research & Development Foundation for the Independent States of the Former Soviet Union (CRDF). This work is partly based on data obtained with the G.D. Cassini Telescope, operated in Loiano (Italy) by the Osservatorio Astronomico di Bologna. GMS is grateful to S. Bernabei, A. De Blasi, and R. Gualandi for assistance with the observations at Loiano. This work was partly supported by the Italian Ministry for University and Research (MURST) under grant Cofin 98-02-32 and by the Italian Space Agency under contract ASI I/R/27/00. Part of this work was supported by the TMR research network “Accretion onto black holes, compact stars, and protostars” funded by the European Commission under contract number ERBFMRX-CT98-0195. Skinakas Observatory is a collaborative project of the University of Crete, the Foundation for Research and Technology-Hellas, and the Max-Planck-Institut für extraterrestrische Physik. We are grateful to Neal Yasami for assistance with the Nebraska observations, and to Laura Gaskell for assistance with the CCD system on the 0.4-meter. SK acknowledges financial support by the Colton Scholarships, and AVF is grateful for a Guggenheim Foundation Fellowship.

REFERENCES

- Abramowicz, M.A., Czerny, B., Losota, J.P., & Szuszkiewicz, E. 1988, *ApJ*, 332, 646
- Alexander, T. 1997, in *Astronomical Time Series*, ed. D. Maoz, A. Sternberg, & E.M. Liebowitz (Dordrecht: Kluwer), 163
- Boller, T., Brandt, W.N., & Fink, H. 1996, *A&A*, 305, 53
- Boller, T., Brandt, W.N., Fabian, A.C., & Fink, H.H. 1997, *MNRAS*, 289, 393
- Boroson, T.A., & Green, R.F. 1992, *ApJS*, 80, 109
- Cardelli, J.A., Clayton, G.C., & Mathis, J.S. 1989, *ApJ*, 345, 245
- Collier, S. et al. 2001, *ApJ*, in press (astro-ph/0107059; Paper II)
- Done, C., Ward, M.J., Fabian, A.C., Kunieda, H., Tsuruta, S., Lawrence, A., Smith, M.G., & Wamsteker, W. 1990, *MNRAS*, 243, 713
- Edelson, R. et al. 2000, *ApJ*, 534, 180
- Edelson, R., Turner, T.J., Pounds, K.A., Vaughan, S., Markowitz, A., Marshall, H., Dobbie, P., & Warwick, R. 2001, in preparation
- Gaskell, C.M., & Sparke, L.S. 1986, *ApJ*, 305, 175
- Kaspi, S. et al. 1996, *ApJ*, 470, 336
- Kaspi, S., Smith, P.S., Netzer, H., Maoz, D., Jannuzi, B.T., & Givon, U. 2000, *ApJ*, 533, 631
- Landolt, A. 1992, *AJ*, 104, 340
- Maoz, D., Edelson, R., & Nandra, K. 2000, *AJ*, 119, 119
- Miller, H.R., Ferrara, E.C., McFarland, J.P., Wilson, J.W., Daya, A.B., & Fried, R.E. 2000, *NewAR*, 44, 539
- Mineshige, S., Kawaguchi, T., Takeuchi, M., & Hayashida, K. 2000, *PASJ*, 52, 499
- Netzer, H. et al. 1996, *MNRAS*, 279, 429
- Netzer, H., & Davidson, K. 1979, *MNRAS*, 187, 871
- Osterbrock, D.E., & Pogge, R.W. 1985, *ApJ*, 297, 166
- Peterson, B.M., Wanders, I., Horne, K., Collier, S., Alexander, T., Kaspi, S., & Maoz, D. 1998, *PASP*, 110, 660
- Peterson, B.M. et al. 2000, *ApJ*, 542, 161
- Pounds, K.A., Edelson, R., Markowitz, A., & Vaughan, S. 2001, *ApJ*, 550, L15
- Schlegel, D.J., Finkbeiner, D.P., & Davis, M. 1998, *ApJ*, 500, 525
- Stern, B.E., Poutanen, J., Svensson, R., Sikora, M., & Begelman, M.C. 1995, *ApJ*, 449, L13
- Stirpe, G.M. 1990, *A&AS*, 85, 1049
- Taniguchi, Y., Murayama, T., & Nagao, T. 1999, *ApJ*, submitted (astro-ph/9910036)
- Turner, T.J., George, I.M., Nandra, K., & Turcan, D. 1999a, *ApJ*, 524, 667
- Turner, T.J., George, I.M., & Netzer, H. 1999b, *ApJ*, 526, 52
- Turner, T.J., Romano, P., George, I.M., Edelson, R., Collier, S.J., Mathur, S., & Peterson, B.M. 2001, *ApJ*, in press (astro-ph/0105283; Paper I)
- van Groningen, E., & Wanders, I. 1992, *PASP*, 104, 700
- Walter, R., & Fink, H.H. 1993, *A&A*, 274, 105
- White, R.J., & Peterson, B.M., 1994, *PASP*, 106, 879
- Young, A.J., Crawford, C.S., Fabian, A.C., Brandt, W.N., & O’Brien, P.T. 1999, *MNRAS*, 304, L46